




Evidence of a second-order phase transition in the six-dimensional Ising spin glass in a fieldM. Aguilar-Janita *Complex Systems Group, Universidad Rey Juan Carlos, 28933 Móstoles, Madrid, Spain*V. Martin-Mayor *Departamento de Física Teórica, Universidad Complutense, 28040 Madrid, Spain
and Instituto de Biocomputación y Física de Sistemas Complejos (BIFI), 50018 Zaragoza, Spain*J. Moreno-Gordo *Instituto de Biocomputación y Física de Sistemas Complejos (BIFI), 50018 Zaragoza, Spain;
Departamento de Física Teórica, Universidad de Zaragoza, 50009 Zaragoza, Spain;
Departamento de Física, Universidad de Extremadura, 06006 Badajoz, Spain;
and Instituto de Computación Científica Avanzada (ICCAEx), Universidad de Extremadura, 06006 Badajoz, Spain*J. J. Ruiz-Lorenzo *Departamento de Física, Universidad de Extremadura, 06006 Badajoz, Spain;
Instituto de Computación Científica Avanzada (ICCAEx), Universidad de Extremadura, 06006 Badajoz, Spain;
and Instituto de Biocomputación y Física de Sistemas Complejos (BIFI), 50018 Zaragoza, Spain*

(Received 8 June 2023; accepted 5 April 2024; published 10 May 2024)

The very existence of a phase transition for spin glasses in an external magnetic field is controversial, even in high dimensions. We carry out massive simulations of the Ising spin-glass in a field, in six dimensions (which, according to classical—but not generally accepted—field-theoretical studies, is the upper critical dimension). We obtain results compatible with a second-order phase transition and estimate its critical exponents for the simulated lattice sizes. The detailed analysis performed by other authors of the replica symmetric Hamiltonian, under the hypothesis of critical behavior, predicts that the ratio of the renormalized coupling constants remain bounded as the correlation length grows. Our numerical results are in agreement with this expectation.

DOI: [10.1103/PhysRevE.109.055302](https://doi.org/10.1103/PhysRevE.109.055302)**I. INTRODUCTION**

The existence of a spin-glass (SG) transition in the presence of an external magnetic field, at the so-called de Almeida-Thouless (dAT) line [1], is one of the most challenging problems in the realm of disordered systems [2–5]. The existence of the dAT line is firmly established only in the limit of infinite space dimensions, $D \rightarrow \infty$ [2].

In order to clarify this problem, the community has tried to implement the Wilson renormalization group (RG) program [6,7]. The starting point is the computation of the so-called upper critical dimension D_u (the smallest D at which critical exponents take their Gaussian values). Unfortunately, this approach, extremely successful in an enormous variety of problems including SG at zero field [8,9], has not yet succeed. Replicated field theory finds $D_u = 6$, but fails to find, in the one-loop approximation, a fixed point stable at $D = 6$ [10,11]. In fact, we identify no fewer than eight conflicting scenarios:

(i) The droplets model predicts the absence of a dAT line for any $D < \infty$ (i.e., the so-called *lower* critical dimension is $D_l = \infty$) [12–15].

(ii) A modified version of the droplets model finds $D_u = D_l = 6$. In other words, a SG phase transition would be possible in a field only if $D > 6$ [16]. See also Refs. [17] and [18].

(iii) An analysis based in the study of high-temperature series finds a second phase transition only for $D \geq 6$ [19].

(iv) A very recent field-theoretical analysis claims $D_u = 8$ [20].

(v) Interestingly enough, a two-loop computation does find a nontrivial stable fixed point at $D = 6$ [21,22], the Gaussian one being unstable. This nontrivial fixed-point would lie in the nonperturbative region (which makes it unclear whether or not the fixed point would survive a three-loops computation).

(vi) The scenario described in Ref. [23] predicts a quasi-first-order transition in a field.

(vii) Large-scale numerical simulations suggest the presence of a dAT line for $D=4$ [24], but the results are not conclusive for $D=3$ [25,26].

(viii) The study of $D=1$ models with long-range interactions that mimic short-range models at $D > 1$ provides somewhat contradicting results. Some studies argue that there must not be a dAT line below $D=6$ [27–29], while others claim in favor of a dAT line for much lower D [30,31].

Here we add clarity to the debate by showing numerical evidence that a dAT line is present in $D=6$ through massive numerical simulations: our largest lattices contain 8^6 spins, more than twice the 48^3 spins in the largest system ever equilibrated in $D=3$ [32]. We find that the scaling behavior of the different susceptibilities is qualitatively different from their zero field counterpart. We have also been able to estimate the critical exponents. However, the lack of analytical predictions for the logarithmic corrections of the different observables

and the size of our statistical errors prevent us from making any strong claim regarding the value of D_0 . Finally, we obtain numerical evidence that the two-parameter replica symmetric (RS) effective Hamiltonian [11] is able to describe the scaling of the ratio of the renormalized coupling constants in the critical region, which enables us to discuss the problem of a second-order phase transition versus a quasi-first-order one.

The structure of the paper is as follows. First, we describe our model (Sec. II), the field-theoretical framework (Sec. II A), and the finite-size scaling techniques (Sec. II B) used to study it. Then we present our numerical results in Sec. III. In particular, in this section we briefly introduce the details of our simulations (Sec. III A), and we study the replicon and anomalous susceptibilities (Sec. III B), the probability density function of the overlap (Sec. III C), the critical exponents (Sec. III D), and the parameter λ (Sec. III E). Finally, we discuss our results and draw some conclusions in Sec. IV.

The paper is supplemented by eight Appendixes, organized as follows. In Appendix A we present the effective Hamiltonian and the structure of the propagators. In Appendix B we revisit theoretical results pertaining to the Helmholtz and Gibbs free energies. Appendix C is dedicated to defining the parameter λ_r and the study of its estimators. Details of our simulations and algorithms are presented in Appendix D and Appendix E. Appendix F address the computation of the critical exponents. In Appendix G we present numerical results for the $h = 0$ phase transition of the six-dimensional Ising spin glass. We conclude by studying the Λ cumulants in Appendix H.

II. THE MODEL

We consider the Edwards-Anderson Hamiltonian for Ising spins (i.e., $s_x = \pm 1$) on a six-dimensional cubic lattice of size $V = L^6$, with periodic boundary conditions and nearest-neighbor interactions:

$$\mathcal{H} = - \sum_{\langle x,y \rangle} J_{xy} s_x s_y - h \sum_x s_x, \quad (1)$$

where the couplings are independent, identically distributed random variables ($J_{xy} = \pm 1$ with equal probability). Hereafter, the overline $\overline{(\dots)}$ means average over the couplings, and $\langle \dots \rangle$ is the thermal average carried out for fixed couplings $\{J_{xy}\}$. A choice of couplings is named a *sample*.

A. Field-theoretical framework

The analysis of the RS Hamiltonian in the field theory (see Appendix A) finds three masses (replicon, anomalous, and longitudinal) and their associated propagators (correlation functions) [11,33]. In the spin-glass phase, the most singular mode is the replicon. The anomalous and longitudinal modes become identical when one takes the limit for the number of replicas n going to zero. Hence the two fundamental propagators of the theory, $G_R(\mathbf{x} - \mathbf{y})$ and $G_A(\mathbf{x} - \mathbf{y})$, are defined as (see Appendix A for more details)

$$G_R(\mathbf{x} - \mathbf{y}) = \overline{\langle s_x s_y \rangle^2} - 2 \overline{\langle s_x s_y \rangle \langle s_x \rangle \langle s_y \rangle} + \overline{\langle s_x \rangle^2 \langle s_y \rangle^2} \quad (2)$$

and

$$G_A(\mathbf{x} - \mathbf{y}) = \overline{\langle s_x s_y \rangle^2} - 4 \overline{\langle s_x s_y \rangle \langle s_x \rangle \langle s_y \rangle} + 3 \overline{\langle s_x \rangle^2 \langle s_y \rangle^2}. \quad (3)$$

Associated with each two-point correlation functions one can define a susceptibility χ as

$$\chi_\alpha = \widehat{G}_\alpha(\mathbf{0}) \quad \alpha \in \{R, A\}, \quad (4)$$

where $\widehat{G}(\mathbf{k})$ is the discrete Fourier transform of $G(\mathbf{x})$ [see Eq. (A6)]. In the $h = 0$ case, it is straightforward to show that $\chi_R = \chi_A = \chi_L$. When $h \neq 0$ instead, we shall find below that χ_R becomes dominant in the spin-glass phase.

In order to study the RS effective Hamiltonian, one introduces ω_1 and ω_2 , which are the following three-point connected correlation functions at zero external momentum:

$$\omega_1 = \frac{1}{V} \sum_{xyz} \overline{\langle s_x s_y \rangle_c \langle s_y s_z \rangle_c \langle s_z s_x \rangle_c}, \quad (5)$$

$$\omega_2 = \frac{1}{2V} \sum_{xyz} \overline{\langle s_x s_y s_z \rangle_c^2}, \quad (6)$$

where the c subindices stand for *connected* correlation functions. We refer the reader to Appendixes B and C for the technical details about the computation of ω_1 and ω_2 .

An interesting observable is the ratio of the two renormalization vertices of the theory, denoted $w_{1,r}$ and $w_{2,r}$:

$$\lambda_r = \frac{w_{2,r}}{w_{1,r}}. \quad (7)$$

Interestingly enough, this ratio can be easily obtained as well (see Appendix C for additional details) in terms of ω_1 and ω_2 as

$$\lambda_r = \frac{\omega_2}{\omega_1}. \quad (8)$$

This equation allows us to compute the ratio of the two renormalized couplings (λ_r) in a numerical simulation on the lattice by computing the quotient of two connected correlations functions at zero external momentum.

Finally, let us remark that there are two different ways of taking the limits for $\lambda_r(L, T)$ at T_c :

$$\lambda_r^* = \lim_{L \rightarrow \infty} \lim_{T \rightarrow T_c} \lambda_r(L, T), \quad \lambda_r(T_c^+) = \lim_{T \rightarrow T_c^+} \lim_{L \rightarrow \infty} \lambda_r(L, T). \quad (9)$$

In principle, $\lambda_r^* \neq \lambda_r(T_c^+)$. We are interested in $\lambda_r(T_c^+)$ [34].

Notice that six real replicas (six independent copies of the system evolving under the same couplings) are needed to compute ω_1 and ω_2 . However, one can compute ω_1 and ω_2 in terms of three and four real-replica estimators (see Appendix C). Within the framework of the RS theory [33], the values of the three- and four-replica estimators differ in general from the true values of ω_1 and ω_2 but coincide with them at the critical temperature. This gives us the opportunity to check the validity of the RS theory by computing the six-, four-, and three-replica estimators [35].

Another check is the value of λ_r itself, since the replica symmetric field theory predicts a value of $0 \leq \lambda_r \leq 1$ for a second-order phase transition while a value of $\lambda_r > 1$ would imply the presence of a quasi-first-order phase transition [23]. It is worth noting that λ_r controls as well the mean-field (MF) values of equilibrium and off-equilibrium dynamical exponents [33].

B. Finite-size scaling

We want to investigate whether or not the systems undergoes a second-order phase transition in the presence of a magnetic field and, if the answer is positive, to characterize the resulting universality class. Indeed, a standard way of identifying a phase transition is computing some correlation length ξ that is used to identify scale invariance. An appropriate definition of the second-moment correlation length in a finite lattice is [7]

$$\xi_2 = \frac{1}{2 \sin(\pi/L)} \left(\frac{\widehat{G}_R(0)}{\widehat{G}_R(\mathbf{k}_1)} - 1 \right)^{1/2}, \quad (10)$$

where $\mathbf{k}_1 = (2\pi/L, 0, 0, 0, 0, 0)$ (or permutations). The scale invariance of ξ_2/L at the critical point results in

$$\frac{\xi_2}{L} = f_\xi(L^{1/\nu}t) + L^{-\omega} g_\xi(L^{1/\nu}t) + \dots, \quad (11)$$

where ω is the correction-to-scaling exponent and $t = (T - T_c)/T_c$ is the reduced temperature. From this behavior one expects that a plot of $\xi_2(T)/L$ for several system sizes will show a common intersection point at $T = T_c$, provided that the sizes are large enough to make corrections to scaling negligible. However, previous works in lower dimensions [24,30] did not find this intersection. This anomalous behavior was attributed to an abnormal behavior of the propagator at wave vector $\mathbf{k} = \mathbf{0}$ [30], which induces strong corrections to the leading scaling behavior in Eq. (11). This phenomenon is illustrated through the spin-glass order parameter distribution in Sec. III C.

Given the aforementioned anomaly, we consider a second scale-invariant quantity, previously introduced in Ref. [24] under the name R_{12} , which is computed as a dimensionless ratio of propagators with higher momenta

$$R_{12} = \frac{\widehat{G}_R(\mathbf{k}_1)}{\widehat{G}_R(\mathbf{k}_2)}. \quad (12)$$

Here \mathbf{k}_1 and \mathbf{k}_2 are the smallest nonzero momenta compatible with periodic boundary conditions, namely, $\mathbf{k}_1 = (2\pi/L, 0, 0, 0, 0, 0)$ and $\mathbf{k}_2 = (2\pi/L, \pm 2\pi/L, 0, 0, 0, 0)$ (and permutations). Notice that R_{12} scales in the same way as ξ_2/L ; see Eq. (11).

III. NUMERICAL RESULTS

In this section we present the numerical results obtained from our simulations. We begin by briefly describing our simulations. Subsequently, we delve into the study of the susceptibilities, the probability density function of the overlap, the critical exponents, and the parameter λ_r .

A. Description of simulations

We have studied the model in Eq. (1) through Monte Carlo simulations on lattices $L = 5, 6, 7$, and 8 , with a magnetic field set to $h = 0.075$. Thermalization is ensured by using the parallel tempering algorithm [36,37], complemented with a demanding equilibration test based on Ref. [38]. In order to obtain high statistics, we have simulated 25 600 samples for $L = 5, 6, 7$ and 5120 for the largest lattice size $L = 8$ by using

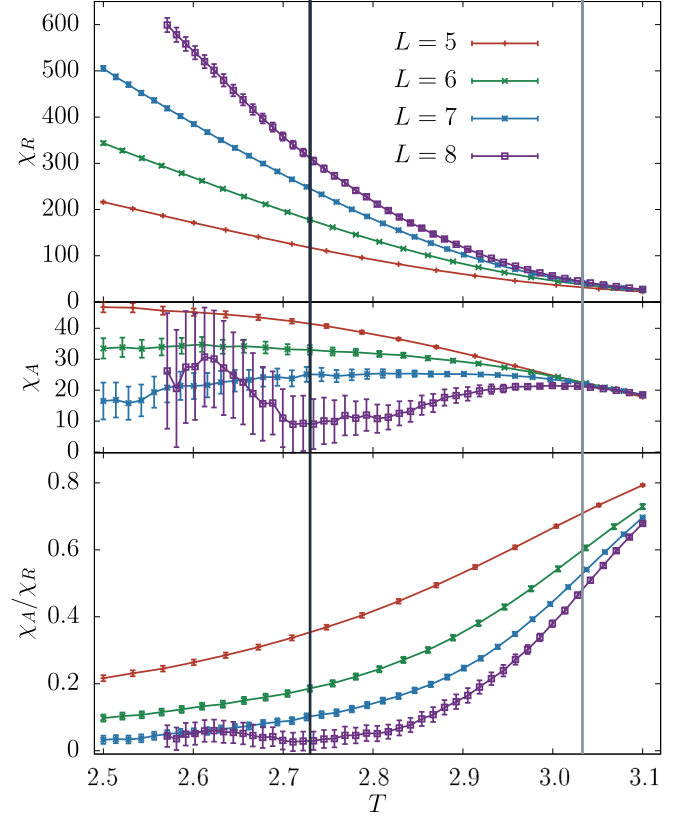


FIG. 1. Susceptibilities for the replicon χ_R (on the top), Eqs. (2) and (4), for the anomalous mode χ_A (on the middle), Eqs. (3) and (4), and for the ratio of the anomalous mode and the replicon one, χ_A/χ_R , (on the bottom), vs temperature T , as computed for our different system sizes in a magnetic field $h = 0.075$. For $h = 0$ one trivially shows that $\chi_R = \chi_A$. Instead, for $h = 0.075$, we find that χ_R rapidly grows with L at low temperatures, while χ_A/χ_R goes to zero. The different size dependence ensures that we are working far enough from the $h = 0$ point in the dAT line. The two vertical lines are our estimates for the critical temperatures for $h = 0.075$ (left vertical line) and for $h = 0$ (right line). In particular, note from the middle panel that the values of χ_A , as computed in $L = 7$ and 8 lattices, are compatible: i.e., differences smaller than two standard deviations at, and below, our estimated critical temperature for $h = 0.075$.

multispin coding. Six statistically independent system copies of each sample, named real replicas, are simulated in order to compute without statistical bias both ω_1 and ω_2 ; recall Eqs. (5) and (6). Further details about our simulations are provided in Appendixes D and E.

B. Replicon and anomalous susceptibilities

One may question if our magnetic field $h = 0.075$ is large enough to ensure that we are working far enough from the $h = 0$ endpoint of the dAT line. We answer that question by computing the replicon and anomalous susceptibilities: notice that for $h = 0$, $\chi_A = \chi_R$. In Fig. 1 we represent χ_R (top panel), χ_A (middle panel), and the ratio χ_A/χ_R (bottom panel). Indeed, at the critical point even our smallest system $L = 5$ has $\chi_R(L = 5, T_c) \approx 3 \chi_A(L = 5, T_c)$, and this ratio gets larger as L grows (see bottom panel in Fig. 1) [39], meaning that

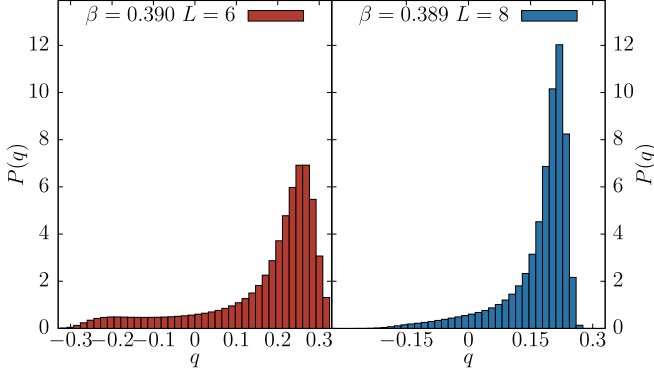


FIG. 2. Probability density function of the overlap $P(q)$ for two different sizes: $L = 6$ (left) and $L = 8$ (right). We have computed $P(q)$ for the lowest available temperature for $L = 8$ ($\beta \approx 0.389$) and the closest available temperature for $L = 6$ ($\beta \approx 0.390$).

correlations extend to a much longer distance for the replicon mode than for the anomalous one, in agreement with both the MF picture and previous computations in $D = 3$ [25] and $D = 4$ [40].

C. Probability density function of the overlap

We have computed the probability density function of the overlap, q , for $L = 6$ and $L = 8$. We observe (see Fig. 2) for both lattice sizes that the probability density function is nonzero for negative overlaps. Note that the tail at $q < 0$ is suppressed in the thermodynamic limit. Indeed, the trend towards a suppression of the tail as L grows is very clear from our data in Fig. 2.

As mentioned in the previous section, the non-negligible tail of negative overlaps is probably responsible of the undesirable behavior of the propagator at wave vector $\mathbf{k} = \mathbf{0}$, which makes it difficult to find intersections of the curves corresponding to different (small) lattice sizes of ξ_2/L as a function of temperature.

D. Critical exponents

We start by determining the value of the critical temperature at which the phase transition takes place. Equation (11) tells us that the curves of dimensionless magnitudes such as ξ_2/L and R_{12} , when computed for different system sizes, will intersect at $T_c(h)$. These intersections are shown in Fig. 3 and in Table I. Corrections to scaling cause the intersection points to vary, depending on the considered pair of lattice (L_1, L_2) and the quantity under inspection, ξ_2/L or R_{12} . However, for our largest systems ($L_1 = 7, L_2 = 8$) we find compatible crossings for ξ_2/L and R_{12} . Also the ($L_1 = 6, L_2 = 7$) crossing for

TABLE I. Temperatures for the crossing points of ξ/L and R_{12} for consecutive sizes.

L_1	L_2	T_c^ξ	T_c^R
5	6	2.892(6)	2.680(14)
6	7	2.809(16)	2.739(15)
7	8	2.69(4)	2.74(2)

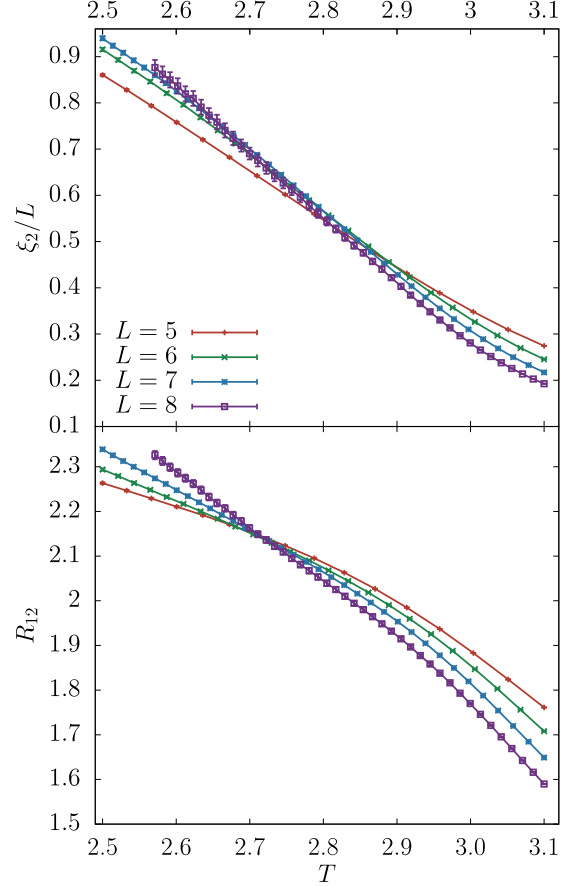


FIG. 3. Second-moment correlation length ξ_2 , Eq. (10), measured in units of the lattice size L (on the top), and dimensionless ratio R_{12} , Eq. (12) (on the bottom), as a function of temperature T . Both quantities are shown as computed for the replicon propagator, Eq. (2), for all our lattice sizes at $h = 0.075$. At the critical point, the curves for different sizes of the system intersect at the same T , meaning that both ξ/L and R_{12} are scale invariant at T_c . The presence of a crossing point for ξ_2/L indicates that the anomalous behavior of the wave vector $\mathbf{k} = \mathbf{0}$ is less severe in space dimension $D = 6$ than previously found at $D = 4$ [24]. The difference between the crossing points found for both quantities should vanish as $L \rightarrow \infty$, since it is due to scaling corrections.

R_{12} turns out to be compatible with the results from ($L_1 = 7, L_2 = 8$). Although a more accurate estimation of T_c is obtained below, the reader can already appreciate that $T_c(h = 0.075)$ is significantly smaller than its $h = 0$ counterpart $T_c(h = 0) = 3.033(1)$ [41,42]. See also Appendix G.

Our next step is the characterization of the universality class by computing critical exponents ν (associated with the correlation length) and η (associated with the replicon susceptibility). We extract effective, size-dependent exponents by using the quotient method [43–45] (see Table II). To avoid the somewhat problematic $\mathbf{k} = \mathbf{0}$ wave vector we compute ν from the scaling of $\partial R_{12}/\partial T$ (see Appendix F) and η from the susceptibility \mathcal{F} :

$$\mathcal{F} = \widehat{G}_R(\mathbf{k}_1). \quad (13)$$

The effective exponents in Table II need to be extrapolated to $L_1 \rightarrow \infty$. We have checked that these extrapolations

TABLE II. Effective exponents η and ν as obtained from the quotient method for lattices (L_1, L_2) . Values are shown at the temperatures obtained from the crossings in R_{12} .

L_1	L_2	$\eta(T_c^R)$	$\nu(T_c^R)$
5	6	0.40(1)	0.88(7)
6	7	0.28(1)	0.76(5)
7	8	0.21(1)	0.54(6)

are compatible with MF values, $\nu = 1/2$ and $\eta = 0$. We have started with independent fits to the laws $\nu(L_1) = 1/2 + O(L_1^{-\omega_\nu})$ and $\eta(L_1) = O(L_1^{-\omega_\eta})$ obtaining good fits, where ω_i ($i = \nu, \eta$) is the leading correction-to-scaling exponent [46]. For ν we get $\chi^2/\text{dof} = 2.9/1$ (dof is the number of degrees of freedom) with a p value = 9% and $\omega_\nu = 3.7(1.3)$. For η we obtain $\chi^2/\text{dof} = 0.03/1$ with a p value = 87% and $\omega_\eta = 1.93(15)$. We can improve by trying a joint fit for ν and η that assumes a common value of $\omega_{\nu\eta}$ (in agreement with the RG expectation). The joint fit obtains $\omega_{\nu\eta} = 1.96(15)$ with $\chi^2/\text{dof} = 5.67/3$ with a p value = 13%. Our extrapolations to large L_1 not constrained to yield MF exponents resulted in exceedingly large errors for both ν and η . Thus, although our estimated exponents are compatible with an upper critical dimension in a field $D_u^h = 6$, we cannot exclude nearby values for D_u^h . In particular, the largeness of the ω exponent seems in contradiction with the logarithmic corrections (i.e., $\omega = 0$) expected at the upper critical dimension.

At this point, we are ready for a joint extrapolation to infinite system sizes of the critical temperature. With the data appearing in Table I, we perform a joint fit with the two data sets to

$$\beta_c^L = \beta_c^\infty + A \frac{s^{-\omega} - 1}{1 - s^{1/\nu}} L^{-\omega - 1/\nu}, \quad (14)$$

where $\beta = 1/T$, $s = (L + 1)/L$, $\omega = 5(2)$, and ν is fixed to $\nu = 1/2$. The results of the fit are $T_c = 1/\beta_c^\infty = 2.755(13)$ with $\chi^2/\text{dof} = 5.02/2$ with a p value = 8.0%.

We have also checked that the impact of the factor $f(s) = (s^{-\omega} - 1)/(1 - s^{1/\nu})$ is negligible. Actually, if we perform the same fit setting $f(s) = 1$ we obtain $T_c = 1/\beta_c^\infty = 2.755(15)$ with $\chi^2/\text{dof} = 5.48/2$ with a p value = 6.5%.

E. Study of the λ_r parameter

Finally, let us consider the λ_r parameter from Eq. (8), that we have computed using the three-, four-, and six-replica estimators of ω_1 and ω_2 . These multiple calculations enable us to check two predictions from the RS theory. First, it predicts that the three and four replicas estimators give the true value of λ_r (which is the one of the six-replica estimator) near the critical point. Second, this theory predicts a value of $\lambda_r \in [0, 1]$. The two following subsections address these points.

1. Comparison of λ_r computed with three, four, and six replicas

We represent in Fig. 4 the three-, four-, and six-replica estimator of λ_r for different lattice sizes $L = 6, 7$, and 8 (bottom, middle, and top panels, respectively). We also plot

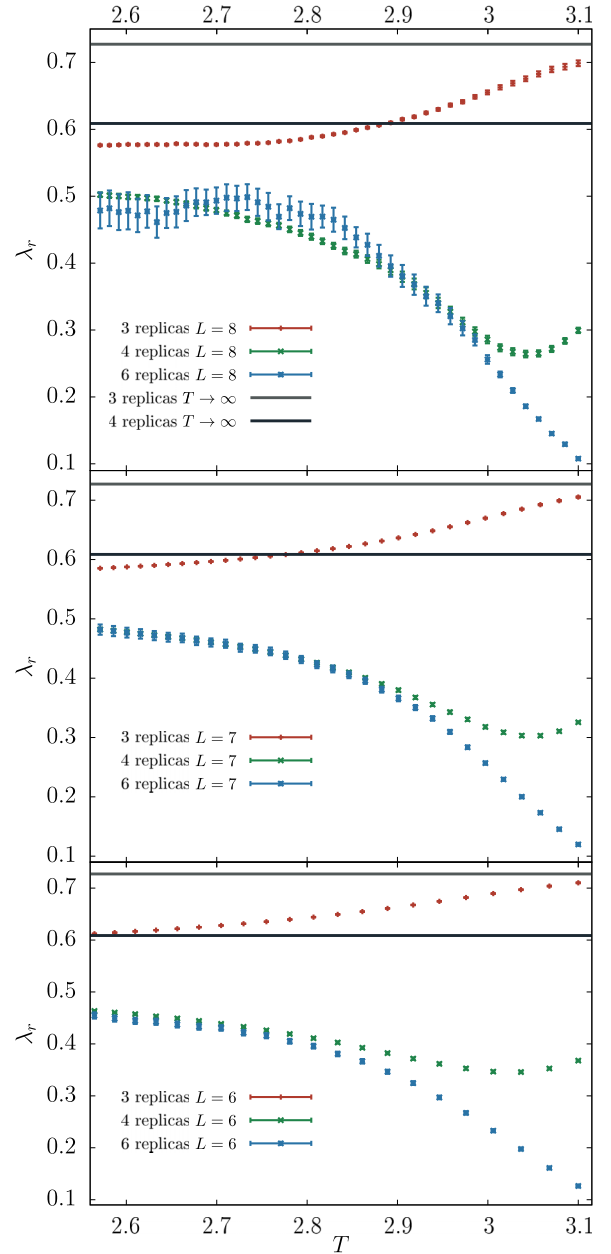


FIG. 4. Plot of the three-, four-, and six-replica estimator of λ_r , Eqs. (C7), (C8), and (B9), respectively, as a function of the temperature for $L = 6$ (bottom panel), for $L = 7$ (middle panel), and for $L = 8$ (top panel). We also plot the infinite temperature limits for three and four replicas.

the infinite temperature values for three and four replicas. The three-replica estimator seems to converge to the infinite value faster than the four-replica estimator, which exhibits a crossover between the six-replica behavior at low temperatures and the infinite temperature one at higher temperatures. Note that, at the estimated critical temperature $T_c = 2.755(13)$, the four- and six-replica estimators are compatible within one standard deviation. Thus, we will use the four-replica estimator which exhibits a smaller statistical error.

In Fig. 5 we show the values of six-replica estimator of λ_r as a function of the temperature for different lattice sizes.

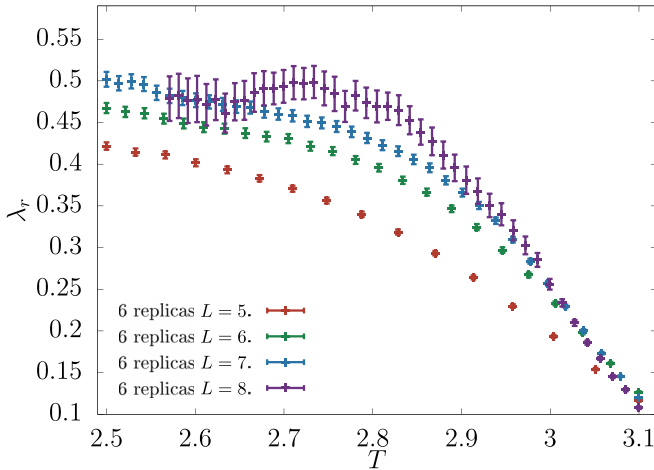


FIG. 5. Plot of the six-replica estimator of λ_r , Eq. (B9) and (C5), as a function of the temperature for all the lattice sizes L .

2. Value of $\lambda_r(T_c^+)$

The validity of the prediction of $\lambda_r \in [0, 1]$ can be addressed from Fig. 6 (we employ dark colors for the values of λ_r computed with three replicas and light colors for the four-replica estimator). Notice that the scaling corrections of the three- and four-replica estimators have opposite signs. Hence we can assume that $\lambda_r(T_c^+)$ lies between the three- and four-replica estimate of λ_r for our largest lattice at our estimate of the critical point. In this way, we conclude that $\lambda_r(T_c^+) = 0.52(6)$.

IV. CONCLUSIONS

We have found numerical evidences for a second-order phase transition in the six-dimensional Ising spin glass in an external field by using state-of-the-art techniques for the Monte Carlo simulations and for the data analysis. We have also performed a first computation of the critical exponents

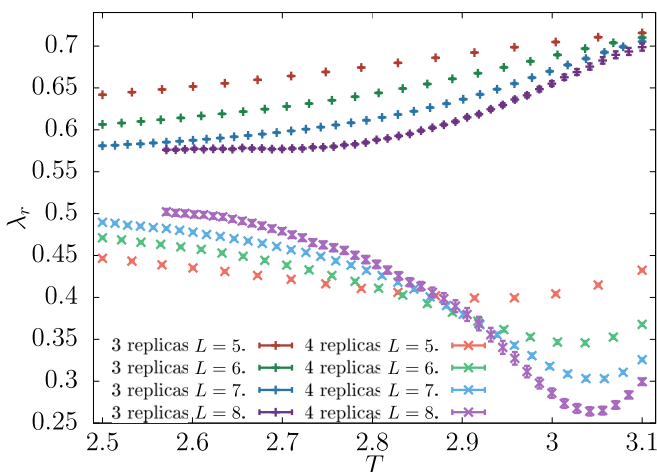


FIG. 6. Three- and four-replica estimators of λ_r , Eqs. (C7) and (C8), as a function of the temperature. The six-replica estimator, shown in Appendix C, turned out to be compatible with—but much noisier than—the four-replica estimator.

for this phase transition. Our finding of a second-order phase transition in six dimensions in a field corroborates, and complements, the analysis based on high-temperature series expansions by Singh and Young [19].

The difficulty in interpreting this finding lies in the absence of a stable fixed point in the one-loop studies for this problem based in the renormalization group by Bray and Roberts [10], which opens the doors to nonperturbative scenarios. In fact, a recent study (conducted up to second order in perturbation theory) has found an additional and stable fixed point [21,22]. Furthermore, in Ref. [20] it has been claimed that the upper critical dimension is eight (rather than six). Our findings are most easily interpreted in this context. An scenario in which a nonperturbative fixed point appears below eight dimensions, which controls the second-order phase transition in six dimensions, seems quite natural.

However, we should stress that both techniques have their own limitations: truncation of the series in the case of the high-temperature expansions and the impossibility to simulate very large lattices in the case of numerical simulations. As a consequence, both techniques could miss a crossover to a different behavior that would appear at higher orders in the series expansion, or for larger systems in the case of the simulations. This could be a crossover to a quasi-first-order transition scenario [23] or even to a no-phase transition scenario [12–16]. If present, this change of behavior should occur at a crossover length larger than our simulated sizes $L = 8$. We are unaware of quantitative estimates of this crossover length in the literature. We should stress, however, that in the absence of a field (when there is no doubt that six is the upper critical dimension) our simulated sizes $L \simeq 8$ are enough for a characterization of the phase transition, including its associated logarithmic corrections; see Ref. [41] and Appendix G.

Let us conclude by stating that we consider that additional analytical and numerical studies are needed to fully understand the intriguing challenge of characterizing the critical behavior of a spin glass in a field in finite dimensions.

ACKNOWLEDGMENTS

Our simulations have been carried out in the ADA cluster at the the Instituto de Computación Científica Avanzada de Extremadura (ICCAEx) at Badajoz and at the Cierzo cluster at the Instituto de Biocomputación y Física de Sistemas Complejos (BIFI) in Zaragoza. We would like to thank both institutions and their staff. This work was partially supported by Ministerio de Ciencia, Innovación y Universidades (Spain), Agencia Estatal de Investigación (AEI, Spain, 10.13039/501100011033), and European Regional Development Fund (ERDF, A Way of Making Europe) through Grants No. PID2020-112936GB-I00 and PID2022-136374NB-C21, by the Junta de Extremadura (Spain), and Fondo Europeo de Desarrollo Regional (FEDER, EU) through Grant No. IB20079. M.A.-J. was supported by the Community of Madrid and Rey Juan Carlos University through the Young Researchers program in R&D (Grant No. CCASSE M2737). J.M.-G. was supported by the Ministerio de Universidades and the European Union “NextGenerationEU/PRTR” through a 2021–2023 Margarita Salas grant.

APPENDIX A: THE HAMILTONIAN AND THE STRUCTURE OF THE PROPAGATORS

The effective Hamiltonian describing the critical behavior of the D -dimensional Ising spin-glass model in presence of a magnetic field h can be written using the replica framework as [11]

$$\mathcal{H} = \frac{1}{2} \int d^D x \left[\frac{1}{2} \sum_{ab} (\nabla \phi_{ab})^2 + m_1 \sum_{ab} \phi_{ab}^2 + m_2 \sum_{abc} \phi_{ab} \phi_{ac} + m_3 \sum_{abcd} \phi_{ab} \phi_{cd} - \frac{1}{6} \tilde{w}_1 \sum_{abc} \phi_{ab} \phi_{bc} \phi_{ca} - \frac{1}{6} \tilde{w}_2 \sum_{ab} \phi_{ab}^3 \right], \quad (\text{A1})$$

where the replicated overlap, ϕ_{ab} , is a $n \times n$ symmetric matrix with zero in the diagonal and n is the number of replicas ($n \rightarrow 0$).

The three fundamental modes of the correlation function are named replicon, anomalous, and longitudinal modes. The anomalous and longitudinal modes become identical when one takes the limit of vanishing n . The fundamental propagators of the theory $G_R(\mathbf{x} - \mathbf{y})$ and $G_A(\mathbf{x} - \mathbf{y})$ are related to the natural propagators $G_1(\mathbf{x} - \mathbf{y})$, $G_2(\mathbf{x} - \mathbf{y})$, and $G_3(\mathbf{x} - \mathbf{y})$ as

$$\begin{aligned} G_R(\mathbf{x} - \mathbf{y}) &= G_1(\mathbf{x} - \mathbf{y}) - 2G_2(\mathbf{x} - \mathbf{y}) + G_3(\mathbf{x} - \mathbf{y}), \\ G_A(\mathbf{x} - \mathbf{y}) &= G_L(\mathbf{x} - \mathbf{y}) = G_1(\mathbf{x} - \mathbf{y}) - 4G_2(\mathbf{x} - \mathbf{y}) \\ &\quad + 3G_3(\mathbf{x} - \mathbf{y}), \end{aligned} \quad (\text{A2})$$

where

$$G_1(\mathbf{x} - \mathbf{y}) = \overline{\langle s_x s_y \rangle^2} - q^2, \quad (\text{A3})$$

$$G_2(\mathbf{x} - \mathbf{y}) = \overline{\langle s_x s_y \rangle \langle s_x \rangle \langle s_y \rangle} - q^2, \quad (\text{A4})$$

$$G_3(\mathbf{x} - \mathbf{y}) = \overline{\langle s_x \rangle^2 \langle s_y \rangle^2} - q^2, \quad (\text{A5})$$

with, as usual, $q = \overline{\langle s_x \rangle^2}$ being the average overlap.

The Fourier transform of the correlation functions is

$$\hat{G}_\alpha(\mathbf{k}) = \sum_r e^{i\mathbf{k}\cdot\mathbf{r}} G_\alpha(\mathbf{r}), \quad \alpha \in \{1, 2, 3, R, L, A\}. \quad (\text{A6})$$

Associated with each two-point correlation functions one can define a susceptibility χ_α as

$$\chi_\alpha = \hat{G}_\alpha(\mathbf{0}), \quad \alpha \in \{1, 2, 3, R, L, A\}. \quad (\text{A7})$$

In the particular case of $h = 0$ case one finds $\chi_R = \chi_A = \chi_L$ (because $\chi_2 = \chi_3 = 0$). However, as soon as $h \neq 0$, the replicon χ_R becomes significantly larger than $\chi_A = \chi_L$ in the spin-glass phase. Details on how to compute the correlation functions with a multispin coding algorithm can be found in Appendix D.

APPENDIX B: THE HELMHOLTZ AND GIBBS FREE ENERGIES

With this Hamiltonian we can compute the associated free energy, the Helmholtz one, defined as

$$F(\lambda_{ab}) = -\frac{1}{V} \ln \langle e^{\sum_{(ab)} V \lambda_{ab} \delta \tilde{Q}_{ab}} \rangle_r, \quad (\text{B1})$$

where (ab) denotes sum over $a \neq b$, the average over the replicated system is denoted as $\langle (\dots) \rangle_r$ (see Ref. [33]) and

$$\delta \tilde{Q}_{ab} \equiv Q_{ab} - q, \quad (\text{B2})$$

with

$$Q_{ab} \equiv \frac{1}{V} \sum_x s_x^a s_x^b. \quad (\text{B3})$$

This free energy allows us to compute the average value of the overlap

$$\langle \delta \tilde{Q}_{ab} \rangle_r = -\frac{\partial F}{\partial \lambda_{ab}}. \quad (\text{B4})$$

The Gibbs free energy, $G(\delta Q_{ab})$, is just the Legendre transform of $F(\lambda_{ab})$ given by

$$G(\delta Q_{ab}) = F(\lambda_{ab}) + \sum_{ab} \lambda_{ab} \delta Q_{ab}, \quad (\text{B5})$$

λ_{ab} being a function of δQ_{ab}

$$\lambda_{ab} = \frac{\partial G}{\partial \delta Q_{ab}}. \quad (\text{B6})$$

The Taylor expansion of the Helmholtz free energy (up to third order) is

$$\begin{aligned} F(\lambda) &= -\frac{1}{2} \sum_{(ab)(cd)} G_{ab,cd} \lambda_{ab} \lambda_{cd} \\ &\quad - \frac{1}{6} \sum_{(ab),(cd),(ef)} \mathcal{W}_{ab,cd,ef} \lambda_{ab} \lambda_{cd} \lambda_{ef}. \end{aligned} \quad (\text{B7})$$

The coefficients $\mathcal{W}_{ab,cd,ef}$ can take only eight different values in a RS phase, namely, $\mathcal{W}_{ab,bc,ca} = \mathcal{W}_1$, $\mathcal{W}_{ab,ab,ab} = \mathcal{W}_2$, $\mathcal{W}_{ab,ab,ac} = \mathcal{W}_3$, $\mathcal{W}_{ab,ab,cd} = \mathcal{W}_4$, $\mathcal{W}_{ab,ac,bd} = \mathcal{W}_5$, $\mathcal{W}_{ab,ac,ad} = \mathcal{W}_6$, $\mathcal{W}_{ac,bc,de} = \mathcal{W}_7$, and $\mathcal{W}_{ab,cd,ef} = \mathcal{W}_8$.

In terms of these \mathcal{W}_i ($i = 1, \dots, 8$) the cubic part of the Helmholtz free energy can be written as

$$\begin{aligned} &\sum_{(ab),(cd),(ef)} \mathcal{W}_{ab,cd,ef} \lambda_{ab} \lambda_{cd} \lambda_{ef} \\ &= \omega_1 \sum_{abc} \lambda_{ab} \lambda_{bc} \lambda_{ca} + \omega_2 \sum_{ab} \lambda_{ab}^3 + \omega_3 \sum_{abc} \lambda_{ab}^2 \lambda_{ac} \\ &\quad + \omega_4 \sum_{abcd} \lambda_{ab}^2 \lambda_{cd} + \omega_5 \sum_{abcd} \lambda_{ab} \lambda_{ac} \lambda_{bd} + \omega_6 \sum_{abcd} \lambda_{ab} \lambda_{ac} \lambda_{ad} \\ &\quad + \omega_7 \sum_{abcde} \lambda_{ac} \lambda_{bc} \lambda_{de} + \omega_8 \sum_{abcdef} \lambda_{ab} \lambda_{cd} \lambda_{ef}. \end{aligned} \quad (\text{B8})$$

We quote here only the relationship between ω_1 and ω_2 (the two relevant terms in this context [33]) and the \mathcal{W}_i [47]:

$$\begin{aligned}\omega_1 &= \mathcal{W}_1 - 3\mathcal{W}_5 + 3\mathcal{W}_7 - \mathcal{W}_8, \\ \omega_2 &= \frac{1}{2}\mathcal{W}_2 - 3\mathcal{W}_3 + \frac{3}{2}\mathcal{W}_4 + 3\mathcal{W}_5 + 2\mathcal{W}_6 - 6\mathcal{W}_7 + 2\mathcal{W}_8.\end{aligned}\quad (\text{B9})$$

that can expressed as

$$\begin{aligned}\omega_1 &= \frac{1}{V} \sum_{xyz} \overline{\langle s_x s_y \rangle_c \langle s_y s_z \rangle_c \langle s_z s_x \rangle_c}, \\ \omega_2 &= \frac{1}{2V} \sum_{xyz} \overline{\langle s_x s_y s_z \rangle_c^2},\end{aligned}\quad (\text{B10})$$

where by $\langle (\dots) \rangle_c$ we denote connected correlation functions. Notice that the coefficients of the terms of order $O(\lambda^m)$ in the expansion of the Helmholtz free energy, $F(\lambda)$, are the m term connected susceptibilities.

At this point the Gibbs free energy can be written as

$$\begin{aligned}G(\delta Q) &= \frac{1}{2} \sum_{(ab),(cd)} \delta Q_{ab} M_{ab,cd} \delta Q_{cd} \\ &\quad - \frac{w_1}{6} \sum_{abc} \delta Q_{ab} \delta Q_{bc} \delta Q_{ca} - \frac{w_2}{6} \sum_{ab} \delta Q_{ab}^3.\end{aligned}\quad (\text{B11})$$

Observe that the cubic coupling in the Hamiltonian are written as \tilde{w}_1 , \tilde{w}_2 , and they are different from the coefficients w_1 , w_2 of the Gibbs free energy [33] (the so-called vertices in field theoretical language). The coefficients \tilde{w}_i and w_i are, respectively, the bare and dressed couplings, The bare and dressed couplings generally differ; they are equal only at the level of the tree approximation in field theory.

APPENDIX C: DETAILS FOR THE COMPUTATION OF THE PARAMETER λ_r IN NUMERICAL SIMULATIONS

A good way to study the nature of the transition is by means of the parameter λ_r defined as

$$\lambda_r = \frac{w_{2,r}}{w_{1,r}}, \quad (\text{C1})$$

where $w_{1,r}$ and $w_{2,r}$ are the renormalized exact vertices of the static replicated Gibbs free energy [33] defined in terms of the connected correlation functions computed at zero momenta as [48]

$$w_{i,r} = \frac{\omega_i}{\chi_R^{3/2} \xi_2^{D/2}} \quad (i = 1, 2). \quad (\text{C2})$$

Therefore

$$\lambda_r = \frac{w_{2,r}}{w_{1,r}} = \frac{\omega_2}{\omega_1}. \quad (\text{C3})$$

In addition, it can be shown that the exact vertices (w_i) can be expressed in terms of the connected correlations functions at zero momenta (ω_i) as [33]

$$w_i = \frac{\omega_i}{\chi_R^3} \quad (i = 1, 2) \quad (\text{C4})$$

and so

$$\lambda_r = \frac{w_{2,r}}{w_{1,r}} = \frac{\omega_2}{\omega_1} = \frac{w_2}{w_1}. \quad (\text{C5})$$

Notice that the parameter λ_r is also related with the cubic couplings \tilde{w}_1 and \tilde{w}_2 of the replica symmetric Hamiltonian of Bray and Roberts [10] since, at the mean-field (MF) level, we have $\tilde{w}_i = w_i$ ($i = 1, 2$). Then, $\lambda_r < 1$ signals the breaking point from RS to replica symmetry breaking [49]. Let us finally remark that all microscopic models, each of them with its own λ_r parameter at a general temperature, will display the same $T \rightarrow T_c$ limit for $\lambda_r = w_{2,r}/w_{1,r}$. Indeed, in Parisi's renormalization scheme both $w_{1,r}$ and $w_{2,r}$ are universal, i.e., independent of the microscopic Hamiltonian [48].

In numerical simulations we compute ω_1 and ω_2 using Eq. (B9) with the \mathcal{W}_i given by [33]

$$\begin{aligned}\mathcal{W}_1 &\equiv V^2 \overline{\langle \delta \tilde{Q}_{12} \delta \tilde{Q}_{23} \delta \tilde{Q}_{31} \rangle}, \\ \mathcal{W}_2 &\equiv V^2 \overline{\langle \delta \tilde{Q}_{12}^3 \rangle}, \\ \mathcal{W}_3 &\equiv V^2 \overline{\langle \delta \tilde{Q}_{12}^2 \delta \tilde{Q}_{13} \rangle}, \\ \mathcal{W}_4 &\equiv V^2 \overline{\langle \delta \tilde{Q}_{12}^2 \delta \tilde{Q}_{34} \rangle}, \\ \mathcal{W}_5 &\equiv V^2 \overline{\langle \delta \tilde{Q}_{12} \delta \tilde{Q}_{13} \delta \tilde{Q}_{24} \rangle}, \\ \mathcal{W}_6 &\equiv V^2 \overline{\langle \delta \tilde{Q}_{12} \delta \tilde{Q}_{13} \delta \tilde{Q}_{14} \rangle}, \\ \mathcal{W}_7 &\equiv V^2 \overline{\langle \delta \tilde{Q}_{12} \delta \tilde{Q}_{13} \delta \tilde{Q}_{45} \rangle}, \\ \mathcal{W}_8 &\equiv V^2 \overline{\langle \delta \tilde{Q}_{12} \delta \tilde{Q}_{34} \delta \tilde{Q}_{56} \rangle},\end{aligned}\quad (\text{C6})$$

and the overlap fluctuations $\delta \tilde{Q}_{ab}$ can be computed in terms of independent real replicas (a and b) using Eq. (B2).

To compute each cubic cumulant \mathcal{W}_i requires a number of different real replicas equal to the largest index in its expression. The RS field theory predicts that the amplitudes of the $\{\mathcal{W}_1, \dots, \mathcal{W}_8\}$ set are not independent [33]. Using the linear relationship between them one can compute ω_1 and ω_2 in terms of three- and four-replica estimators. In particular, the three-replica estimators are [33]

$$\omega_1^{(3)} \equiv \frac{11}{30} \mathcal{W}_1 + \frac{2}{15} \mathcal{W}_2, \quad \omega_2^{(3)} \equiv \frac{4}{15} \mathcal{W}_1 - \frac{1}{15} \mathcal{W}_2, \quad (\text{C7})$$

and the four-replica ones [33]

$$\begin{aligned}\omega_1^{(4)} &\equiv \frac{23\mathcal{W}_1}{30} + \frac{\mathcal{W}_2}{20} - \frac{3\mathcal{W}_3}{5} + \frac{9\mathcal{W}_4}{20} - \frac{6\mathcal{W}_5}{5} + \frac{\mathcal{W}_6}{2}, \\ \omega_2^{(4)} &\equiv \frac{7\mathcal{W}_1}{15} + \frac{2\mathcal{W}_2}{5} - \frac{9\mathcal{W}_3}{5} + \frac{3\mathcal{W}_4}{5} - \frac{3\mathcal{W}_5}{5} + \mathcal{W}_6.\end{aligned}\quad (\text{C8})$$

Within the framework of the RS theory, the values of the three- and four-replica estimators differ in general from the true values of ω_1 and ω_2 but coincide with them at the critical temperature [33]. This gives us the opportunity to check the validity of the RS theory by computing the three-, four-, and six-replica estimators.

1. λ_r infinite-temperature limit

As a part of our analysis of the behavior of the observable λ_r , we have studied how far from the infinite-temperature limit our results are. In this section we show the computations of λ_r in the infinite-temperature limit for three, four, and six replicas.

Actually, the computation of λ_r at infinite temperature is reduced to the computation of the cubic cumulants \mathcal{W}_i with $i \in \{1, 2, \dots, 8\}$ in the same regime.

Let us start by computing the very simple case of the cumulant \mathcal{W}_2 . Starting from the expression of the cumulant given by Eq. (C6) and Eq. (B2) we can develop the expression of \mathcal{W}_2 :

$$\mathcal{W}_2 = V^2 \langle (\overline{Q_{12}} - q)^3 \rangle = V^2 \langle \overline{Q_{12}^3} \rangle - 3q \langle \overline{Q_{12}^2} \rangle + 2V^2 q^3. \quad (\text{C9})$$

In the infinite-temperature limit in which we are interested of, the value of q tends to 0, so the only relevant term is $V^2 \langle \overline{Q_{12}^3} \rangle$. Expanding this term we get

$$\langle \overline{Q_{12}^3} \rangle = \frac{1}{V^3} \sum_{xyz} \langle s_x^1 s_x^2 s_y^1 s_y^2 s_z^1 s_z^2 \rangle. \quad (\text{C10})$$

In the infinite-temperature limit, the only relevant terms are those with $x = y = z$. Other possibilities vanish when thermal averages are taken since thermal fluctuations are dominant in that regime. Thus, we have

$$\langle \overline{Q_{12}^3} \rangle_{T \rightarrow \infty} = \frac{1}{V^3} \sum_x \langle s_x^1 s_x^2 s_x^1 s_x^2 s_x^1 s_x^2 \rangle. \quad (\text{C11})$$

Spins appearing an odd number of times lead to cancellations in the Eq. (C11) when thermal averages are taken. On the contrary, spins appearing an even number of times can pair each other and contribute one unit to the sum.

This simple reasoning indicate us that, each time a replica is appearing an odd number of times in the expression of \mathcal{W}_i , that cubic cumulant will be 0 in the infinite-temperature limit. That is the case for \mathcal{W}_i with $i \geq 2$. However, for \mathcal{W}_1 we have

$$\mathcal{W}_1 = V^2 \langle \overline{Q_{12} Q_{23} Q_{31}} \rangle - 3q \langle \overline{Q_{12} Q_{13}} \rangle + 2V^2 q^3. \quad (\text{C12})$$

In Eq. (C12), the only nonzero term in the infinite limit, the first one, contains an even number of spins of each replica when expanding it. Therefore, this term will contribute with a factor 1 when averages are taken. Then $\mathcal{W}_1 = 1$ and $\mathcal{W}_i = 0$ for $i \geq 2$ in the infinite-temperature limit.

At this point, the computation of λ_r is easy. From Eq. (C1) we obtain

$$\lambda_r = \frac{\omega_2}{\omega_1} = 0. \quad (\text{C13})$$

Similar computations are valid for the three- and four-replica cases. From Eqs. (C7) and Eqs. (C8) we have

$$\lambda_r^{(3)} = \frac{\omega_2^{(3)}}{\omega_1^{(3)}} = \frac{8}{11}, \quad (\text{C14})$$

$$\lambda_r^{(4)} = \frac{\omega_2^{(4)}}{\omega_1^{(4)}} = \frac{14}{23}. \quad (\text{C15})$$

APPENDIX D: NUMERICAL SIMULATION DETAILS

To study the six-dimensional Ising spin glass in the presence of a magnetic field we have written several computer programs in C language. In our simulations, we use an offline analysis approach, meaning our simulation program writes configurations of spins and then a different analysis program computes the correlation lengths and other magnitudes of interest. Finally, a third program is in charge of the statistical

TABLE III. Some parameters of our simulation. The first column refers to the size of the side of the hypercube. In the second column we present the number of samples analyzed. The third column shows the number of temperatures simulated for each size. This number has been chosen in a way that ensures the random walk in temperatures to be sufficiently ergodic. The fourth and fifth columns refer to the lower and upper values of the temperature interval. Finally, the last column shows the number of picoseconds (ps) per spin flip of the simulation.

L	No. samples	No. temp.	T_{\min}	T_{\max}	ps/spin flip
5	25 600	16	2.50	3.10	16
6	25 600	24	2.50	3.10	12
7	25 600	36	2.50	3.10	20
8	5120	44	2.57	3.10	16

analysis of the data, using the Jackknife technique [50,51]. It is worth mentioning that both, the simulation and the analysis program, make use of the POSIX thread libraries, which allow us to create different threads that run parallel on different cores.

We have simulated the Edwards-Anderson model in a six-dimensional hypercube with periodic boundary conditions, using a multispin coding Monte Carlo simulation and performing a parallel tempering [36,37] proposal every 20 Monte Carlo sweeps (MCSs). For each sample, we have simulated six replicas. The sizes of the side L of the hypercube range from $L = 5$ to $L = 8$. The value of the magnetic field h has been set to $h = 0.075$. The number of samples used to obtain the results that we present can be consulted in Table III, along with other information about the simulations.

To ensure that we measure the equilibrium properties of the system, the thermalization of each sample must be studied individually. We have designed a thermalization protocol based on Ref. [38] that works in the following way.

First we simulate our supersample (a package of 128 samples) during a sufficiently large number of MCS for most of the samples to be thermalized. This value \mathcal{N}_{sim} was determined by preliminary runs.

During the simulation, the random walk in temperatures induced by the parallel tempering algorithm for each of the 128 samples is registered. Then, when the simulation ends, we study this random walk and compute from it the integrated autocorrelation time $\tau_{\text{int},f}$ for several magnitudes f , related to the random walks [38]. We take the largest of these integrated autocorrelation times, τ_{int,f^*} , and make the assumption $\tau_{\text{int},f^*} \sim \tau_{\text{exp}}$. The value of the exponential autocorrelation time enables us to check if a given sample is thermalized. In particular, we consider a sample to be thermalized if its simulation time τ_{sim} is 30 times bigger than τ_{exp} (i.e., $\mathcal{N}_{\text{sim}} > 30\tau_{\text{exp}}$).

When in a supersample a nonequilibrated sample is found, we proceed as follows. The last configurations of those samples which are not thermalized are extracted from the corresponding supersample. Then a new supersample is built grouping nonthermalized samples and their simulation time is doubled. Finally, the thermalization check is repeated, τ_{exp} is measured, and if the criteria are not fulfilled, the simulations

are extended once again. This process is repeated until all samples reach their equilibrium states. At the end, the samples are reintroduced into their original supersamples, ready to be analyzed.

APPENDIX E: DETAILS OF MULTISPIN CODING ALGORITHMS

One of the most complex tasks we have faced when trying to generate the results that we present here is the elaboration of coding algorithms. In this Appendix we show some examples that can give a taste of how the problem is approached.

1. Metropolis algorithm

Current CPUs are able to execute one-clock-cycle instructions over registers (or words) of 128 bits. The 128-bit words are coded by using the Intel Intrinsics [52] variables `__m128i` consisting of 128 Boolean variables. We benefit from these 128-bit words by simulating at once 128 samples.

Let us define a vector $S[V]$ of type `__m128i`, where V is the number of spins of our system. Each element of the vector $S[i]$, contains 128 Boolean variables representing the value of the spin at the i th position for the 128 samples. Analogously, we can define a vector $J[6*V]$ in which each element $J[i]$ contains the value of the coupling for the 128 samples at the i th position. Now, the problem reduces to code the Metropolis algorithm in bitwise operations to improve the performance up to 128 times. We work with the following assignment:

$$s = +1 \rightarrow b_s = +1, \text{ and } s = -1 \rightarrow b_s = 0, \quad (\text{E1})$$

$$J = +1 \rightarrow b_J = 0 \text{ and } J = -1 \rightarrow b_J = 1, \quad (\text{E2})$$

where the b variables are the bit variable of our program. This seemingly arbitrary election has a virtue: the equivalence

$$b_{s1} \wedge b_J \wedge b_{s2} = (1 - J s_1 s_2)/2, \quad (\text{E3})$$

where \wedge represents the Boolean *exclusive or* (XOR).

We use a variation from the original Metropolis algorithm to decide if a given spin is flipped or not. The Hamiltonian is composed of an interaction term \mathcal{H}_J and a magnetic field term \mathcal{H}_h . The probability of performing a given spin flip is determined by the product

$$\min\{1, \exp(-\Delta\mathcal{H}_J)\} \min\{1, \exp(-\Delta\mathcal{H}_h)\}. \quad (\text{E4})$$

This election is not completely equivalent to the standard Metropolis algorithm, but it verifies the detailed balance condition and has the virtue of simplifying the implementation. One can execute this spin flip simultaneously for the 128 samples having an `__m128i` variable `flip` which encodes the information. If the spin from the i th sample must be flipped, then `flipi = 1`, if it must remain in the same position `flipi = 0`. Then one can carry out the flip decision simultaneously using the XOR operator

$$S[\text{site}] = S[\text{site}] \wedge \text{flip}[\text{site}]. \quad (\text{E5})$$

The `flip` variable has two different contributions, one coming from the difference in the interaction energy considering the spin neighbors, `flipJ`, and other coming from the spin

alignment with the field h , `fliph`, so that

$$\text{flip} = \text{flipJ} \& \text{fliph} \quad (\text{E6})$$

we denote with `&` the boolean AND operation.

Since we consider only nearest-neighbor interactions this energy difference coming from the interactions with the neighboring sites will be

$$\Delta\mathcal{H}_J = -2s_x \sum_y J_{xy} s_y, \quad (\text{E7})$$

where the sum is restricted over the 12 neighbors of s_x . In the $\{+1, -1\}$ base the energy difference $\Delta\mathcal{H}_J$ can take 12 values ranging from -24 to $+24$ in steps of 4. To compute ΔE_J in the bit base $\{0, 1\}$ we define n_{un} , which represents the number of unsatisfied couplings of a given spin. The maximum possible value of n_{un} is 12, and the energy difference is $\Delta\mathcal{H}_J = 24 - 2n_{\text{un}}$. To compute n_{un} we select a given spin $S[\text{site}]$ and check if a given coupling is satisfied using Eq. (E3). This information is then encoded in eight 128-bit variables. To account for the heat bath effect, we generate a random number $R \in [0, 1)$ and check if $R < \exp(-\beta\Delta\mathcal{H}_J)$ for each sample. We use the same random number for all samples, so we can check if it surpass a barrier of $\exp(-4\beta)$, $\exp(-8\beta)$, \dots , $\exp(-24\beta)$. The number of barriers surpassed is encoded in three new `__m128i` variables named `id1`, `id2`, `id3`. We assign `flipJ` a value of one if

$$\text{id1} + 2\text{id2} + 4\text{id3} + n_{\text{un}} \geq 6. \quad (\text{E8})$$

Computationally, taking this decision takes a total of 54 Boolean operations.

Finally one checks if after the flip the spin is aligned with the field h , and if so make the assignment `fliph = 1`. This process is repeated for every spin of the system.

2. Multispin coding for correlation functions

Our goal is to compute the correlation functions $G_R(x)$ and $G_A(x)$ as defined in Appendix A. For convenience, we define two new propagators Γ_1 and Γ_2 as

$$\Gamma_1(\mathbf{x} - \mathbf{y}) = \overline{(\langle s_x - \langle s_x \rangle \rangle \langle s_y - \langle s_y \rangle \rangle)^2}, \quad (\text{E9})$$

$$\Gamma_2(\mathbf{x} - \mathbf{y}) = \overline{\langle s_x s_y \rangle^2} - \overline{\langle s_x \rangle^2 \langle s_y \rangle^2}. \quad (\text{E10})$$

It can be easily shown that

$$G_R(\mathbf{x} - \mathbf{y}) = \Gamma_1(\mathbf{x} - \mathbf{y}) \quad (\text{E11})$$

and

$$G_A(\mathbf{x} - \mathbf{y}) = 2\Gamma_1(\mathbf{x} - \mathbf{y}) - \Gamma_2(\mathbf{x} - \mathbf{y}), \quad (\text{E12})$$

so it is enough for us to compute Γ_1 and Γ_2 in order to obtain the replicon and anomalous propagators. They can be computed with the help of replicas as

$$\Gamma_1(\mathbf{x} - \mathbf{y}) = \overline{\langle \varphi_{ab;cd}(\mathbf{x}) \varphi_{ab;cd}(\mathbf{y}) \rangle}, \quad (\text{E13})$$

$$\Gamma_2(\mathbf{x} - \mathbf{y}) = \overline{\langle \Delta_{ab;cd}(\mathbf{x}) \Delta_{ab;cd}(\mathbf{y}) \rangle}, \quad (\text{E14})$$

where

$$\varphi_{ab;cd}(\mathbf{x}) = \frac{(s_x^a - s_x^b)(s_x^c - s_x^d)}{2}, \quad (\text{E15})$$

$$\Delta_{ab;cd}(\mathbf{x}) = \frac{(q_x^{ab} - q_x^{cd})}{\sqrt{2}}. \quad (\text{E16})$$

Notice that one needs at least four replicas to compute the two point connected correlation functions estimators. We would like to evaluate the fields $\varphi_{ab;cd}(x)$ and $\Delta_{ab;cd}(x)$ simultaneously for the 128 systems, so we are forced to do it just using Boolean operations. One can easily check that $\varphi_{ab;cd}(x)/2$ can take three values: $+1, 0, -1$. Then its value can be completely determined using three auxiliary Boolean variables defined as

$$\varphi_1 = (s^a \wedge s^b) \& (s^c \wedge s^d), \quad (\text{E17})$$

$$\varphi_2 = (s^a \wedge s^d), \quad (\text{E18})$$

$$\varphi_3 = \varphi_1 \& \varphi_2. \quad (\text{E19})$$

In particular, $\varphi_1 = 1$ if the field in this point $\varphi_{ab;cd}(x)/2$ is not zero and $\varphi_3 = 1$ if it is $+1$. Then one can compute the value of the field in a given hyperplane P using a Boolean sum function and computing

$$\frac{1}{2} \sum_{x \in P} \varphi_{ab;cd}(x) = 2 \sum_{x \in P} \varphi_3(x) - \sum_{x \in P} \varphi_1(x). \quad (\text{E20})$$

To compute $\Delta_{ab;cd}(x)$ one proceeds in a similar way. In particular, the auxiliary Boolean variables are

$$\Delta_1 = (s^a \wedge s^b) \wedge (s^c \wedge s^d), \quad (\text{E21})$$

$$\Delta_2 = \Delta_1 \& (s^c \wedge s^d). \quad (\text{E22})$$

The value of $\Delta_1(x)$ tells you if $\Delta_{ab;cd}(x)/\sqrt{2}$ is $+1$ and Δ_2 if it is not zero.

APPENDIX F: COMPUTING THE CRITICAL EXPONENTS

The value of the critical exponents can be estimated using the quotient method. Usually, the exponent η would be extracted from the replicon susceptibility χ_R , but to avoid the problematic $\mathbf{k} = \mathbf{0}$ wave vector we compute it from \mathcal{F} as defined in Eq. (14), which has the same scaling behavior of χ_R . The quotient method idea is to compute

$$\mathcal{Q}_{\mathcal{F}} = \frac{\mathcal{F}^{L_2}(T_c)}{\mathcal{F}^{L_1}(T_c)} = \left(\frac{L_2}{L_1}\right)^{2-\eta} + \dots, \quad (\text{F1})$$

and then, to leading order,

$$\eta = 2 - \frac{\ln \mathcal{Q}_{\mathcal{F}}}{\ln(L_2/L_1)}. \quad (\text{F2})$$

From our data we can obtain an estimation of η , given the three combinations of increasing values L_1 and L_2 .

The ν exponent can also be computed by using the quotient method. A standard way to do it would be studying the correlation length derivative with respect to the inverse temperature β . However, once again we avoid the $\mathbf{k} = \mathbf{0}$ mode

TABLE IV. Number of samples [independent systems with different values of the interaction coupling J 's, recall Eq. (1)] simulated and the number of MCS made during each simulation for each value of the lattice size L .

L	MCS	No. samples
3	409 600	8500
4	409 600	6500
5	409 600	5500
6	409 600	4000
7	409 600	4000
8	204 800	3000
9	307 200	1000

and compute ν by means of the derivative of the R_{12} , defined in Eq. (13) as

$$\mathcal{Q}_{\partial\beta R} = \frac{\partial_{\beta} R_{12}^{L_2}(T_c)}{\partial_{\beta} R_{12}^{L_1}(T_c)} = \left(\frac{L_2}{L_1}\right)^{1/\nu} + \dots, \quad (\text{F3})$$

$$\nu = \frac{\ln(L_2/L_1)}{\mathcal{Q}_{\partial\beta R}}. \quad (\text{F4})$$

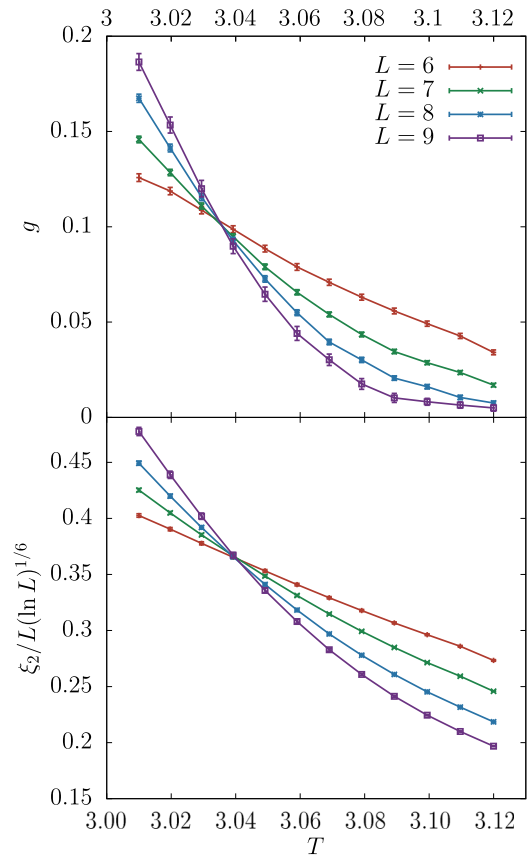


FIG. 7. Binder cumulant g (on the top), Eq. (G2), and the second moment correlation length ξ_2 divided by the lattice size L and by the logarithmic correction term $(\ln L)^{1/6}$ (on the bottom) as a function of temperature for lattice sizes between $L = 6$ and $L = 9$. The presence of an intersection between the curves at temperatures T_c^B and T_c^ξ signals the existence of a continuous phase transition.

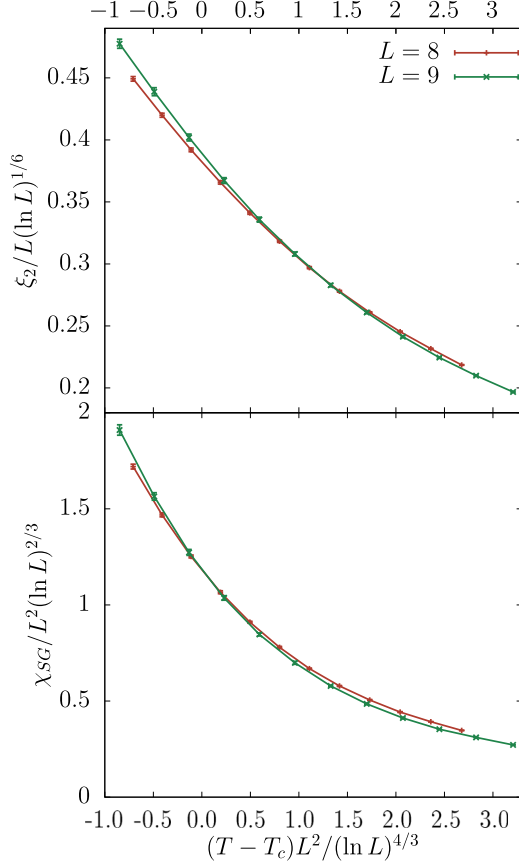


FIG. 8. Second moment correlation length ξ_2 divided by the lattice size L and by the logarithmic correction term $(\ln L)^{1/6}$ (on the top) and the spin-glass susceptibility χ_{SG} divided by $L^{2-\eta}$ (using the mean-field result $\eta = 0$) and by the logarithmic correction term $(\ln L)^{2/3}$ (on the bottom) as a function of the argument of the scaling functions f_ξ and f_χ for lattice sizes $L = 8$ and $L = 9$. Since Eqs. (G9) and (G10) hold asymptotically for large values of L we would expect the two curves to collapse into a single one only if the used values of the logarithmic correction critical exponents \hat{q} and \hat{a} are the correct one.

The values of $\partial_\beta R_{12}$ have been obtained by deriving a polynomial fit of the sixth degree of R_{12} .

APPENDIX G: THE $h = 0$ TRANSITION

1. Theory

As a previous step in the analysis of our system, we have studied the six-dimensional model of an Ising spin glass without a magnetic field, described by the Hamiltonian

$$\mathcal{H} = - \sum_{\langle x,y \rangle} J_{xy} s_x s_y, \quad (\text{G1})$$

where $J_{xy} = \pm 1$ with equal probabilities, s_x are Ising spin variables, and the sum is restricted over nearest neighbors. The system has been studied by means of standard numerical Metropolis Monte Carlo simulations (with a nonmultispin coding program) and the help of the parallel tempering algorithm. We check the existence of a phase transition by

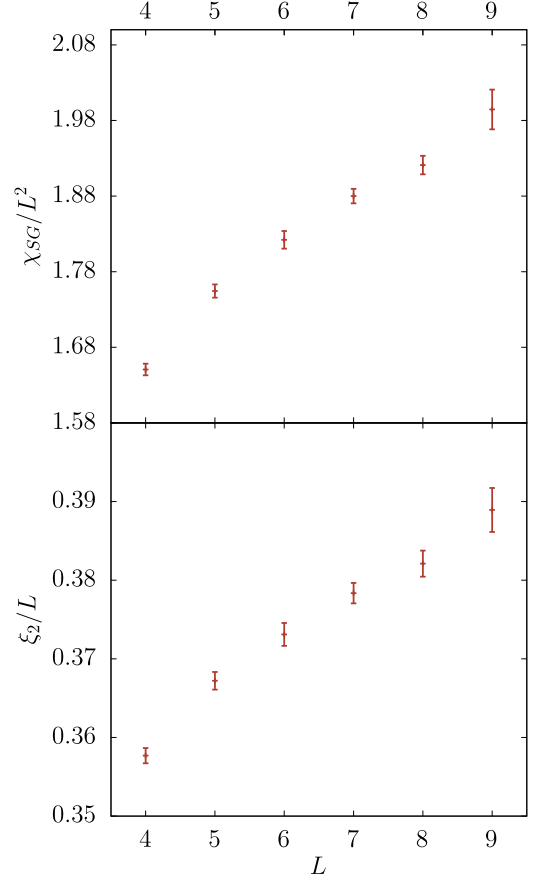


FIG. 9. Plot of $\chi_{SG}(T_c)/L^2$ (on the top) and $\xi_2(T_c)/L$ (on the bottom) vs the lattice size L . The data show a monotonic growth, a strong indication of the presence of logarithmic corrections.

computing the Binder cumulant, defined as

$$g = 1 - \frac{\overline{q_4^2}}{3\overline{q_2^2}^2}, \quad (\text{G2})$$

where the overlap computed in a given sample, q_J , is

$$q_J = \frac{1}{V} \sum_x s_x \tau_x, \quad (\text{G3})$$

where $\{s_x\}$ and $\{\tau_x\}$ are, as usual, two replicas of the system evolving with the same disorder but different initial conditions. The correlation length ξ_2 is defined using the two point (nonconnected) correlation function

$$G(x-y) = \overline{\langle s_x s_y \rangle^2}. \quad (\text{G4})$$

We check the values of the critical exponents, and, since we are at the upper critical dimension D_U , we also check the values of the logarithmic corrections.

In the presence of logarithmic corrections, the scaling laws near the critical point for the correlation length and the susceptibility must be modified as [7,53]

$$\xi_2 \sim |t|^{-\nu} |\ln |t||^{\hat{\nu}}, \quad (\text{G5})$$

$$\chi_{SG} \sim |t|^{-\gamma} |\ln |t||^{\hat{\gamma}}. \quad (\text{G6})$$

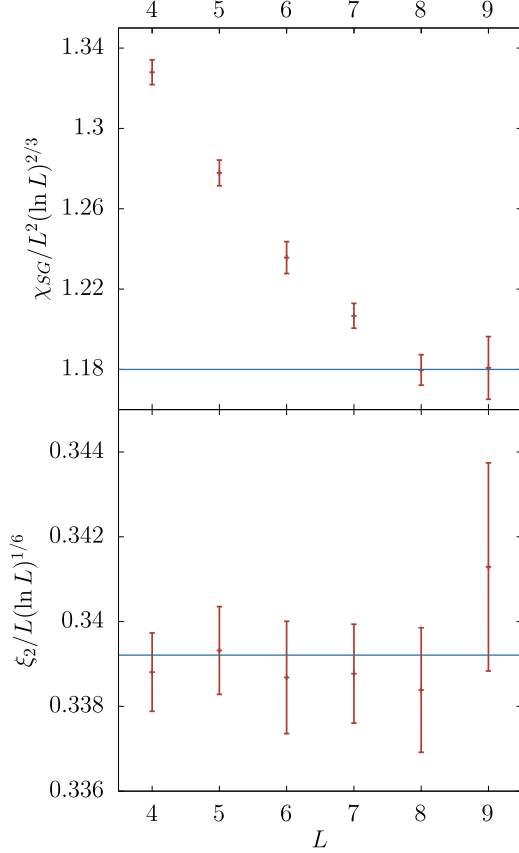


FIG. 10. Plot of $\chi_{SG}(T_c)/[L^2(\ln L)^{2/3}]$ (on the top) and $\xi_2(T_c)/[L(\ln L)^{1/6}]$ (on the bottom) vs the lattice size L . Our data approach asymptotically to a constant value for $L \gg 1$, from which we conclude that they are compatible with the values $\hat{a} = 2/3$ and $\hat{q} = 1/6$. The constant behavior for the bottom plot was expected since the scaling of ξ was used to determine the value of T_c .

At the infinite volume critical point, the correlation length defined on a box of size L behaves as [53]

$$\xi_2 \sim L(\ln L)^{\hat{q}}, \quad (\text{G7})$$

and the susceptibility

$$\chi_{SG} \sim L^{2-\eta}(\ln L)^{\hat{a}}, \quad (\text{G8})$$

so the complete scaling behavior for the six-dimensional spin glass of ξ/L and χ is [54]

$$\xi_2/L = |\ln L|^{\hat{q}} f_{\xi}(L^2 t / (\ln L)^{4/3}) \quad (\text{G9})$$

and

$$\chi_{SG} = L^2 |\ln L|^{\hat{a}} f_{\chi}(L^2 t / (\ln L)^{4/3}), \quad (\text{G10})$$

where we have used the MF values $\nu = 1/2$ and $\eta = 0$. The logarithmic corrections have been computed making use of the renormalization group, and their values are [53–55]: $\hat{q} = 1/6$ and $\hat{a} = 2/3$.

2. Simulation results

We have carried out simulations for systems with size L ranging from $L = 3$ to $L = 9$ and for temperatures between

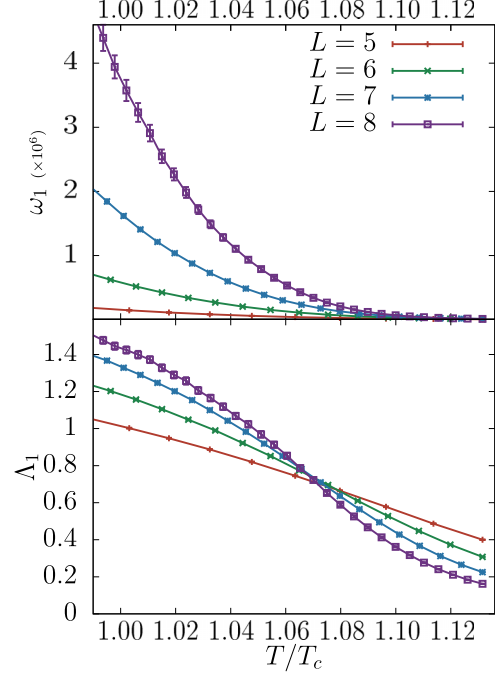


FIG. 11. Plot of ω_1 (on the top), Eq. (B9), and the cumulant Λ_1 (on the bottom), Eq. (H1), as a function of T/T_c .

$T_{\min} = 3.012$ and $T_{\max} = 3.031$. The number of MCS used for each sample as well as the number of samples are reported in Table IV.

The critical temperature have been computed by studying the Binder cumulant and the correlation length (see Fig. 7), and we have obtained a value of

$$T_c = 3.033(1), \quad (\text{G11})$$

which is compatible with the previously known results obtained via simulations $T_c = 3.035(10)$ [41] and a high-temperature expansion $T_c = 3.027(5)$ [42].

The theoretical value of the critical exponents and logarithmic corrections can be checked using the collapse method, i.e., by representing $\xi_2/L |\ln L|^{1/6}$ and $\chi_{SG}/L^{2-\eta} |\ln L|^{2/3}$ vs $L^{1/\nu} t / (\ln L)^{4/3}$. Since the expressions (G9) and (G10) holds asymptotically for large values of L , one would expect the curves for different lattice size to collapse into a single curve near the critical temperature when $L \gg 1$ if and only if the theoretical values of ν , η , \hat{q} , and \hat{a} are the correct ones. The results can be checked in Fig. 8.

Another strong indication of the presence of logarithmic corrections is presented in Fig. 9 in which we plot $\chi_{SG}(T_c)/L^2$ and $\xi_2(T_c)/L$, both showing a clear growth with the lattice size. This behavior was already observed in Ref. [41] for the spin-glass susceptibility and enabled them to estimate the value of the logarithmic correction's power, which was previously unknown at that time.

However, it is difficult to discern with precision the correct value of the logarithmic correction from Fig. 8. Despite this, we can check the outcome of the analytical computation, \hat{q} and \hat{a} , by representing $\chi_{SG}(T_c)/[L^2(\ln L)^{2/3}]$ and $\xi_2(T_c)/[L(\ln L)^{1/6}]$ vs the lattice size L . If the scaling behavior

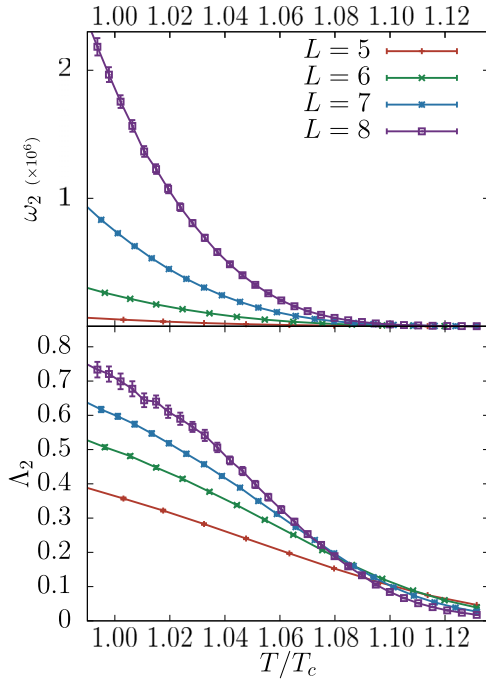


FIG. 12. Up: Plot of ω_2 as a function of T/T_c . Down: Plot of Λ_2 as a function of T/T_c .

(G9) and (G10) holds, and the theoretical values of the critical exponents are compatible with our data, then we would

observe a constant behavior (represented by the blue line in Fig. 10).

From the analysis above, we conclude that our simulation results are compatible with the MF values of the critical exponents and with the theoretical values of the logarithmic corrections $\hat{q} = 1/6$ and $\hat{a} = 2/3$.

APPENDIX H: Λ CUMULANTS

One could have addressed the computation of the two renormalized constants $w_{i,r}$ ($i = 1, 2$), but they present strong finite-size effects. Instead, we have resorted to the computation of the Λ_i cumulants introduced in Ref. [40]:

$$\Lambda_i = \frac{\omega_i}{\chi_R^{3/2} L^{D/2}} \quad \text{with } i \in \{1, 2\}. \quad (\text{H1})$$

The Λ_i cumulants scale in the same way as a dimensionless observable, like the Binder cumulant or ξ_2/L .

In Figs. 11 and 12 one can find a two-panel figure for ω_1 , Λ_1 , and for ω_2 , Λ_2 , respectively, as a function of T/T_c .

Notice that both Λ cumulants show crossing points (better signal for Λ_1), as expected, drifting very slowly to the critical point.

In addition the connected susceptibilities ω_1 and ω_2 diverge in the critical region as predicted by the theory: $\omega_{1,2} \propto |T - T_c|^{-\gamma_3}$ with $\gamma_3 = 6\nu - \frac{3}{2}\nu\eta$ in six dimensions [40] ($\gamma_3 = 3$ for $D = 6$ and the MF exponents).

- [1] J. R. L. de Almeida and D. J. Thouless, Stability of the Sherrington-Kirkpatrick solution of a spin glass model, *J. Phys. A: Math. Gen.* **11**, 983 (1978).
- [2] G. Parisi, M. A. Virasoro, and M. Mézard, *Spin Glass Theory and Beyond* (World Scientific, Singapore, 1987).
- [3] A. P. Young, *Spin Glasses and Random Fields* (World Scientific, Singapore, 1998).
- [4] K. H. Fischer and J. A. Hertz, *Spin Glasses* (Cambridge University Press, Cambridge, 1991).
- [5] E. Bolthausen and A. Bovier, *Spin Glass* (Springer, Berlin, 2007).
- [6] K. G. Wilson and J. Kogut, The renormalization group and the ϵ -expansion, *Phys. Rep.* **12**, 75 (1974).
- [7] D. J. Amit and V. Martin-Mayor, *Field Theory, the Renormalization Group, and Critical Phenomena: Graphs to Computers* (World Scientific, Singapore, 2005).
- [8] A. B. Harris, T. C. Lubensky, and J.-H. Chen, Critical properties of spin-glasses, *Phys. Rev. Lett.* **36**, 415 (1976).
- [9] M. Baity-Jesi, R. A. Baños, A. Cruz, L. A. Fernandez, J. M. Gil-Narvion, A. Gordillo-Guerrero, D. Iñiguez, A. Maiorano, F. Mantovani, E. Marinari *et al.* (Janus Collaboration), Critical parameters of the three-dimensional Ising spin glass, *Phys. Rev. B* **88**, 224416 (2013).
- [10] A. J. Bray and S. A. Roberts, Renormalisation-group approach to the spin glass transition in finite magnetic fields, *J. Phys. C: Solid State Phys.* **13**, 5405 (1980).
- [11] I. R. Pimentel, T. Temesvári, and C. De Dominicis, Spin-glass transition in a magnetic field: A renormalization group study, *Phys. Rev. B* **65**, 224420 (2002).
- [12] W. L. McMillan, Scaling theory of Ising spin glasses, *J. Phys. C: Solid State Phys.* **17**, 3179 (1984).
- [13] D. S. Fisher and D. A. Huse, Ordered phase of short-range Ising spin-glasses, *Phys. Rev. Lett.* **56**, 1601 (1986).
- [14] A. J. Bray and M. A. Moore, Scaling theory of the ordered phase of spin glasses, in *Heidelberg Colloquium on Glassy Dynamics*, Lecture Notes in Physics No. 275, edited by J. L. van Hemmen and I. Morgenstern (Springer, Berlin, 1987), pp. 121–153.
- [15] D. S. Fisher and D. A. Huse, Nonequilibrium dynamics of spin glasses, *Phys. Rev. B* **38**, 373 (1988).
- [16] J. Yeo and M. A. Moore, Critical point scaling of Ising spin glasses in a magnetic field, *Phys. Rev. B* **91**, 104432 (2015).
- [17] M. A. Moore and A. J. Bray, Disappearance of the de Almeida-Thouless line in six dimensions, *Phys. Rev. B* **83**, 224408 (2011).
- [18] G. Parisi and T. Temesvári, Replica symmetry breaking in and around six dimensions, *Nucl. Phys. B* **858**, 293 (2012).
- [19] R. R. P. Singh and A. P. Young, de Almeida–Thouless instability in short-range Ising spin glasses, *Phys. Rev. E* **96**, 012127 (2017).
- [20] M. C. Angelini, C. Lucibello, G. Parisi, G. Perrupato, F. Ricci-Tersenghi, and T. Rizzo, Unexpected upper critical dimension for spin glass models in a field predicted by the loop expansion around the Bethe solution at zero temperature, *Phys. Rev. Lett.* **128**, 075702 (2022).
- [21] P. Charbonneau and S. Yaida, Nontrivial critical fixed point for replica-symmetry-breaking transitions, *Phys. Rev. Lett.* **118**, 215701 (2017).

- [22] P. Charbonneau, Y. Hu, A. Raju, J. P. Sethna, and S. Yaida, Morphology of renormalization-group flow for the de Almeida–Thouless–Gardner universality class, *Phys. Rev. E* **99**, 022132 (2019).
- [23] J. Höller and N. Read, One-step replica-symmetry-breaking phase below the de Almeida–Thouless line in low-dimensional spin glasses, *Phys. Rev. E* **101**, 042114 (2020).
- [24] R. A. Baños, A. Cruz, L. A. Fernandez, J. M. Gil-Narvion, A. Gordillo-Guerrero, M. Guidetti, D. Iñiguez, A. Maiorano, E. Marinari, V. Martín-Mayor *et al.*, Thermodynamic glass transition in a spin glass without time-reversal symmetry, *Proc. Natl. Acad. Sci. USA* **109**, 6452 (2012).
- [25] M. Baity-Jesi, R. A. Baños, A. Cruz, L. A. Fernandez, J. M. Gil-Narvion, A. Gordillo-Guerrero, D. Iñiguez, A. Maiorano, F. Mantovani, E. Marinari, V. Martín-Mayor *et al.*, Dynamical transition in the $D = 3$ Edwards-Anderson spin glass in an external magnetic field, *Phys. Rev. E* **89**, 032140 (2014).
- [26] M. Baity-Jesi, R. A. Baños, A. Cruz, L. A. Fernandez, J. M. Gil-Narvion, A. Gordillo-Guerrero, D. Iñiguez, A. Maiorano, F. Mantovani, E. Marinari, V. Martín-Mayor *et al.*, The three-dimensional Ising spin glass in an external magnetic field: The role of the silent majority, *J. Stat. Mech.* (2014) P05014.
- [27] H. G. Katzgraber and A. P. Young, Probing the Almeida–Thouless line away from the mean-field model, *Phys. Rev. B* **72**, 184416 (2005).
- [28] H. G. Katzgraber, D. Larson, and A. P. Young, Study of the de Almeida–Thouless line using power-law diluted one-dimensional Ising spin glasses, *Phys. Rev. Lett.* **102**, 177205 (2009).
- [29] B. Vedula, M. A. Moore, and A. Sharma, Study of the de Almeida–Thouless line in the one-dimensional diluted power-law XY spin glass, *Phys. Rev. E* **108**, 014116 (2023).
- [30] L. Leuzzi, G. Parisi, F. Ricci-Tersenghi, and J. J. Ruiz-Lorenzo, Ising spin-glass transition in a magnetic field outside the limit of validity of mean-field theory, *Phys. Rev. Lett.* **103**, 267201 (2009).
- [31] M. Dilucca, L. Leuzzi, G. Parisi, F. Ricci-Tersenghi, and J. J. Ruiz-Lorenzo, Spin glasses in a field show a phase transition varying the distance among real replicas (and how to exploit it to find the critical line in a field), *Entropy* **22**, 250 (2020).
- [32] L. A. Fernandez, V. Martín-Mayor, S. Perez-Gaviro, A. Tarancon, and A. P. Young, Phase transition in the three-dimensional Heisenberg spin glass: Finite-size scaling analysis, *Phys. Rev. B* **80**, 024422 (2009).
- [33] G. Parisi and T. Rizzo, Critical dynamics in glassy systems, *Phys. Rev. E* **87**, 012101 (2013).
- [34] In order to compute λ_r^* at the upper critical dimension one could try to adapt to the RS Hamiltonian the strategy followed by Brezin and Zinn-Justin for the ϕ^4 theory [56]. In particular, the theory would be studied from the beginning on a finite box, exactly at its infinite-volume critical temperature. We are not aware of any such computation, not even in the simplest case of the one-component ϕ^3 theory.
- [35] In Ref. [40] the four-dimensional Ising spin glass in a field was analyzed numerically but ω_1 and ω_2 were computed only from three- and four-replica estimators.
- [36] K. Hukushima and K. Nemoto, Exchange Monte Carlo method and application to spin glass simulations, *J. Phys. Soc. Jpn.* **65**, 1604 (1996).
- [37] E. Marinari, Optimized Monte Carlo methods, in *Advances in Computer Simulation*, edited by J. Kerstész and I. Kondor (Springer-Verlag, Berlin, 1998), pp. 57–89.
- [38] A. Billoire, L. A. Fernandez, A. Maiorano, E. Marinari, V. Martín-Mayor, J. Moreno-Gordo, G. Parisi, F. Ricci-Tersenghi, and J. J. Ruiz-Lorenzo, Dynamic variational study of chaos: Spin glasses in three dimensions, *J. Stat. Mech.: Theory Exp.* (2018) 033302.
- [39] One can compare this factor with the values of χ_R/χ_A at $T_c(h = 0)$, which are $\chi_R/\chi_A \simeq 1.35, 1.65, 1.85, 1.96$ for $L = 5, 6, 7$, and 8 respectively.
- [40] L. A. Fernandez, I. Gonzalez-Adalid Pemartin, V. Martín-Mayor, G. Parisi, F. Ricci-Tersenghi, T. Rizzo, J. J. Ruiz-Lorenzo, and M. Veca, Numerical test of the replica-symmetric Hamiltonian for correlations of the critical state of spin glasses in a field, *Phys. Rev. E* **105**, 054106 (2022).
- [41] J. Wang and A. P. Young, Monte carlo study of the six-dimensional Ising spin glass, *J. Phys. A: Math. Gen.* **26**, 1063 (1993).
- [42] L. Klein, J. Adler, A. Aharony, A. B. Harris, and Y. Meir, Series expansions for the Ising spin glass in general dimension, *Phys. Rev. B* **43**, 11249 (1991).
- [43] M. Nightingale, Scaling theory and finite systems, *Physica A* **83**, 561 (1976).
- [44] H. G. Ballesteros, L. A. Fernández, V. Martín-Mayor, and A. Muñoz Sudupe, Finite size effects on measures of critical exponents in $d = 3O(N)$ models, *Phys. Lett. B* **387**, 125 (1996).
- [45] H. G. Ballesteros, L. A. Fernández, V. Martín-Mayor, and A. Muñoz Sudupe, Critical properties of the antiferromagnetic RP^2 model in three dimensions, *Nucl. Phys. B* **483**, 707 (1997).
- [46] Considering only leading corrections to scaling, the quotient of $\partial R_{12}/\partial T$ at the crossing point for (L_1, L_2) is $Q = (L_2/L_1)^{1/\nu} [1 + A_1 L_2^{-\omega}] / [1 + A_1 L_1^{-\omega}]$, where A_1 is an amplitude and ω is the leading corrections-to-scaling exponent. If $L_2 = L_1 + 1$, $Q = (L_2/L_1)^{1/\nu} [1 + A_1 (L_2^{-\omega} - L_1^{-\omega}) + \dots]$. Thus, the exponents we are computing from the fits are $\omega_{\nu, \eta} = \omega + 1$.
- [47] T. Temesvári, C. De Dominicis, and I. Pimentel, Generic replica symmetric field-theory for short range Ising spin glasses, *Eur. Phys. J. B* **25**, 361 (2002).
- [48] G. Parisi, *Statistical Field Theory* (Addison-Wesley, Reading, 1988).
- [49] D. J. Gross, I. Kanter, and H. Sompolinsky, Mean-field theory of the Potts glass, *Phys. Rev. Lett.* **55**, 304 (1985).
- [50] P. Young, *Everything You Wanted to Know about Data Analysis and Fitting but Were Afraid to Ask* (Springer, Cham, 2015).
- [51] B. Efron, *The Jackknife, the Bootstrap, and Other Resampling Plans*, CBMS-NSF Regional Conference Series in Applied Mathematics, Vol. 38 (SIAM, 1982).
- [52] <https://www.intel.com/content/www/us/en/docs/intrinsics-guide/index.html>.
- [53] R. Kenna, D. A. Johnston, and W. Janke, Scaling relations for logarithmic corrections, *Phys. Rev. Lett.* **96**, 115701 (2006).
- [54] J. J. R. Lorenzo, Revisiting (logarithmic) scaling relations using renormalization group, *Condens. Matter Phys.* **20**, 13601 (2017).
- [55] J. J. Ruiz-Lorenzo, Logarithmic corrections for spin glasses, percolation and Lee–Yang singularities in six dimensions, *J. Phys. A: Math. Gen.* **31**, 8773 (1998).
- [56] J. Zinn-Justin, *Quantum Field Theory and Critical Phenomena*, 4th ed. (Clarendon Press, Oxford, 2005).